Journal of Solid State Chemistry 182 (2009) 1846–1855

Contents lists available at ScienceDirect

Journal of Solid State Chemistry

journal homepage: www.elsevier.com/locate/jssc

Incommensurately modulated LT″-$Ni_{1+\delta}Sn$ ($\delta = 0.60, 0.63$): Rietveld refinement, line-broadening analysis and structural relation with LT- and LT′-$Ni_{1+\delta}Sn$

A. Leineweber *

Max Planck Institute for Metals Research, Heisenbergstraße 3, 70569 Stuttgart, Germany

ARTICLE INFO

Article history:
Received 11 January 2009
Received in revised form
24 March 2009
Accepted 18 April 2009
Available online 3 May 2009

Keywords:
Order–disorder phase transitions
Modulated structures
Incommensurate structures
Rietveld refinement
Line-broadening analysis

ABSTRACT

X-ray powder diffraction data of NiAs/Ni_2In-type $Ni_{1.60}Sn$ and $Ni_{1.63}Sn$ alloys annealed at or below about 573 K reveal the development of an incommensurately ordered phase called LT″. In this phase Ni(2) atoms occupy partially the trigonal–bipyramidal interstices formed by five Sn within an NiAs-type arrangement Ni(1)Sn. The modulated occupational ordering of Ni(2) in the LT″ phase can be described in the superspace group $Cmcm(\alpha 00)0s0$, and the parameters describing this occupational modulation were refined together with atomic displacement modulations using the Rietveld method. The structure parameters revealed close structural analogies of the LT″ phase with the previously reported commensurate LT-$Ni_{1+\delta}Sn$ and incommensurate LT′-$Ni_{1+\delta}Sn$ phases (A. Leineweber, J. Solid State Chem. 177 (2004) 1197–1212), which both occur for lower Ni contents than the LT″ phase. The 1st-order satellite reflections visible in the powder-diffraction patterns exhibit, with respect to the fundamental reflections, a considerable diffraction-line broadening, caused by a small *size* of the particularly ordered domains. This small-domain-size broadening was successfully described by a recently developed reflection-index (*hklm*) dependent (anisotropic) line-broadening model (A. Leineweber, V. Petricek, J. Appl. Crystallogr. 40 (2007) 1027–1034) designed to consider the effect of fluctuations of the lattice metrics on the peak widths in powder diffraction patterns of incommensurately modulated crystal structures. The small domain sizes encountered for the LT″ phase indicate that domain coarsening is much more difficult than for the LT and LT′ phases. This special feature of the LT″ phase goes along with a compared to the LT and LT′ phases absent orthorhombic distortion and the low ordering temperature, which are discussed as a consequence of the ordering patterns due to the Ni(2) atoms.

1. Introduction

The Ni–Sn system contains around 40 at% Sn a 'phase region' usually labelled with the formula Ni_3Sn_2. This region comprises a composition range which can be indicated as $Ni_{1+\delta}Sn$ with app. $0.35 < \delta < 0.67$ (maximum extent according to Ref. [1]), and contains different phases having in common that their crystal structures can be derived from the NiAs/Ni_2In-type crystal structure [2,3]: 'Ni(1)Sn' forms a NiAs-type arrangement (the c/a axial ratio is reduced to about 1.26–1.27) with Ni(2) partially occupying trigonal–bipyramidal sites formed by five Sn atoms giving the formula Ni(1)$Ni(2)_\delta$Sn or, in short, $Ni_{1+\delta}Sn$. According to some recent crystal structure work and constitutional investigations [4–7] the above-mentioned 'phase region' encompassing four different phases (Fig. 1): A high-temperature phase HT and three low-temperature phases LT, LT′ and LT″.

The high-temperature phase, HT-$Ni_{1+\delta}Sn$ with $P6_3/mmc$ space-group symmetry (see Fig. 2) forms over the whole above-mentioned composition range without long-range order of Ni(2) on the trigonal–bipyramidal sites. Only short-range order of the Ni(2) atoms occurs [8] together with static displacements of Sn atoms surrounding Ni(2) [6,8].

The HT phase can be retained at room temperature for all compositions by quenching from e.g. 1023 K [5,9]. Three low-temperature phases with ordered arrangement of Ni(2) can form upon slow cooling or, after quenching the HT phase, upon annealing below the strongly composition-dependant order–disorder transition temperature [7]. Until now, detailed crystal-structure data of two of the three low-temperature phases have been reported: The LT phase occurs around the ideal composition Ni_3Sn_2 ($Ni_{1.50}Sn$). The Ni(2) ordering in the LT phase leads to an orthorhombic superstructure having a unit cell with $a_{LT} \approx 2\ a_{HT}$, $b_{LT} \approx 3^{1/2} a_{HT}$, $c_{LT} \approx c_{HT}$ and with $Pbnm$ symmetry [5,10,11]. The LT′

* Fax: +49 711 689 3312.
E-mail address: a.leineweber@mf.mpg.de

0022-4596/$ - see front matter © 2009 Elsevier Inc. All rights reserved.
doi:10.1016/j.jssc.2009.04.019

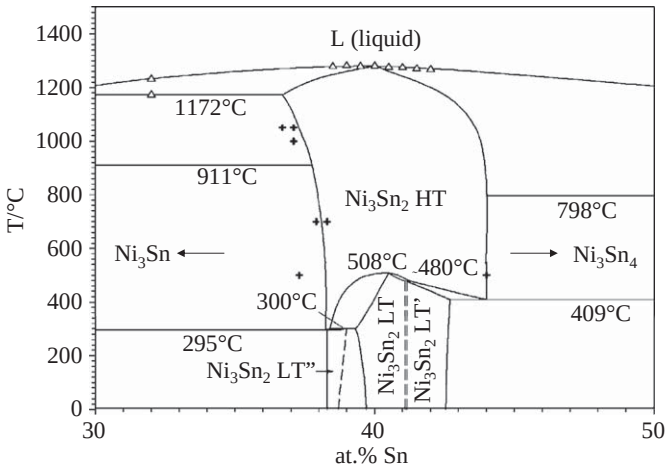

Fig. 1. Phase diagram Ni–Sn around 40 at% Sn considering the differently ordered $Ni_{1+\delta}Sn$ (Ni_3Sn_2) phases [7].

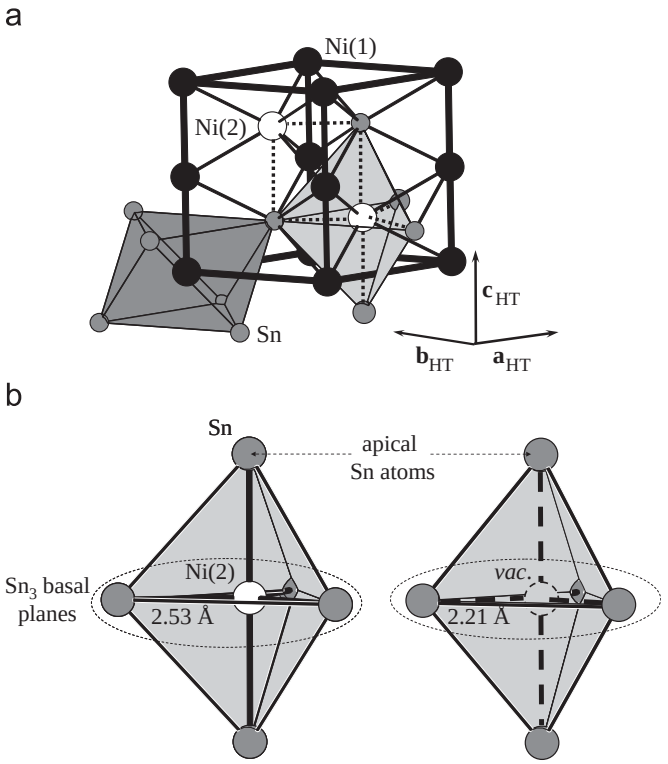

Fig. 2. (a) Crystal-structure principle of the $Ni_{1+\delta}Sn$ ($Ni(1)Ni(2)_\delta Sn$) phases shown on the basis of the hexagonal unit cell of the HT phase: *hcp*-like arrangement of Sn with Ni(1) on all octahedral sites and Ni(2) occupying partially (occupancy of δ) trigonal–bipyramidal 'interstices' formed by five Sn atoms. This occupation is short-range ordered in the HT and long-range ordered in the LT, LT′ and LT″ phases. (b) Sn_5-trigonal bipyramids with expanded Sn_3-basal plane if occupied by Ni(2) (left) and contracted Sn_3-basal plane if empty ('occupied' by vacancy, right). Average distances are given as observed for stoichiometric LT-Ni_3Sn_2 ($Ni_{1.50}Sn$) [5].

phase occurs at the low-Ni content side of the Ni_3Sn_2 phase region ($0.35 \leqslant \delta \leqslant 0.45$, see Fig. 1). This LT′ phase was apparently overlooked (or regarded to be identical to the LT phase) in Ref. [10], and is orthorhombic like the LT phase. The ordering of Ni(2) is incommensurate in the LT′ phase and can be described on the basis of an average lattice with $a_{orth} \approx a_{HT}$, $b_{orth} \approx 3^{1/2} a_{HT}$, $c_{orth} \approx c_{HT}$ and a modulation vector $\mathbf{q} = \alpha \mathbf{a}^*_{orth}$ with the modulation parameter α varying from 0.43 ($\delta = 0.35$) to 0.49 ($\delta = 0.44$) [4]. The superspace-group symmetry was found to be $Cmcm(\alpha 00)0s0$. A closer comparison of the diffraction patterns of the LT and the LT′ phases as well as their structure parameters revealed that the LT phase can be regarded as a commensurately modulated lock-in phase of the LT′-phase with $\mathbf{q} = \alpha \mathbf{a}^*_{orth}/2$ (i.e. $\alpha = \frac{1}{2}$) [4]. For both LT and LT′ phases a dimensionless parameter *orth* can be defined which may be used as a measure for the extent of orthorhombic lattice distortion of the lattice:

$$orth = \frac{b_{orth}}{3^{1/2} a_{orth}} - 1. \quad (1)$$

For both LT and LT′ always $orth > 0$ is found [5].

In this work X-ray powder-diffraction data will be presented characterising the crystal structure of the LT″ phase occurring at the high-Ni content side of the Ni_3Sn_2 phase region in the approximate composition range $Ni_{1.60}Sn$–$Ni_{1.63}Sn$. The main problem of the Rietveld refinement of the crystal structure of LT″-$Ni_{1.60}Sn$ on the basis of these data appeared to be an appropriate description of the considerable line-broadening of the satellite reflections. This problem can be resolved by employing a recently described line-broadening model [15], which has in the meantime already been applied in a case similar to the present one [12]. The similarity of the LT″ with the LT′ and LT phases allows a more general view on the three ordered low-temperature phases in the 'Ni_3Sn_2 phase region', both concerning similarities between all three phases, but also concerning differences between LT″ on the one hand and LT and LT′ phases on the other hand.

2. Experimental

2.1. Preparation

Ni–Sn alloys of the compositions $Ni_{1.60}Sn$ and $Ni_{1.63}Sn$ were prepared as described in Ref. [4] from Ni sheets (99.98 mass%, Goodfellow) and Sn pieces (bars, Heraeus 99.999 mass%). The starting materials were melted by induction heating and cast into water-cooled cylindrical forms of a diameter of 8 mm and a length of 50 mm. The mass of the cast ingots confirmed that there was no significant loss of mass during alloy production. The top and bottom parts of the cast cylinders were removed and the remaining material was sealed in quartz tubes and subjected to a homogenisation treatment of 3 d at 473 K and subsequently 3 d at 1023 K followed by water quenching by crushing the quartz tube. Thereby, a homogeneous bulk specimen of the HT phase was obtained, as evidenced by X-ray diffraction patterns (see Section 2.2). According to Ref [4] results from chemical analysis of alloys as used in this study agree well with the weighted amounts of Ni and Sn used for melting the alloys, therefore the weighted amounts of Ni and Sn were used as the composition of the alloys as given in the following.

Starting from these HT-phase bulk specimens $Ni_{1.60}Sn$ and $Ni_{1.63}Sn$ various isothermal heat treatments were performed to establish differently ordered states:

(i) *Annealing of bulk alloys*: Parts of both the HT-phase bulk specimens $Ni_{1.60}Sn$ and $Ni_{1.63}Sn$ were resealed in quartz tubes and annealed at different annealing temperatures (as indicated in the text) for different periods of time followed by quenching in water including crushing of the quartz tubes.

(ii) *Annealing of alloy powder* (*only* $Ni_{1.60}Sn$): A few grams of the HT-phase bulk specimen $Ni_{1.60}Sn$ were ground in a mortar. The powder was sealed in vacuum into a quartz tube (diameter 3 mm), which was afterwards annealed for 15 min

at 1023 K followed by quenching the tube (without crushing it) in water. Parts of this powder were resealed and subjected to further heat treatments at $T<1023$ K (as indicated in the text) followed by quenching the quartz tube as above.

2.2. X-ray powder diffraction

All X-ray powder-diffraction patterns were recorded on a Philips X'Pert MPD equipped with a Cu tube and a Johannson-type monochromator in the primary beam selecting the $K\alpha 1$ component of the incident radiation.

For measurements suitable for determination of lattice parameters and of the modulation parameter α either the annealed powder was directly used, or the solid alloy was ground in a mortar (either as ground, or mixed with Ge standard powder ($a = 5.6574$ Å)). The powders were fixed using vaseline as a thin layer on a Si wafer cut parallel to a (510) plane.

A measurement suitable for Rietveld refinement (employing JANA2006 [13]) was performed on an annealed-powder sample $Ni_{1.60}Sn$ (10 d at 573 K) using 'back-loaded powder' samples which had a thickness of 0.5 mm and a diameter 10 mm.

3. Results and discussion

3.1. Main phase-transformation effects of HT-$Ni_{1+\delta}$ + Sn ($\delta = 0.60, 0.63$) solid samples and powders upon annealing

Both the bulk alloys and the powder alloys exhibit similar (but slightly different, see what follows) phase-transformation behaviour as a function of the annealing temperature. Note, that, however, in powder-diffraction patterns the powder alloys exhibit narrower reflections than alloys annealed in the bulk state (absence of residual strain due to grinding because of the heat treatment at 1023 K applied to the powder *after* grinding, see Section 2). Thus, e.g. the presence of minority phase reflections is easier detectable for powder alloys than for bulk alloys.

According to the X-ray powder-diffraction patterns, $Ni_{1.60}Sn$ alloy quenched from 1023 K consists of single-phase HT-$Ni_{1+\delta}Sn$, whereas quenched $Ni_{1.63}Sn$ contains small amounts of Ni_3Sn phase. Various heat treatments at $T<1023$ K were performed. The following phenomena were observed:

(a) Bulk and powder samples annealed at and quenched from $623\text{ K}<T<773$ K give rise to X-ray diffraction patterns showing formation of tiny additional amounts of Ni_3Sn (already present for $Ni_{1.63}Sn$ quenched from 1023 K, but not for $Ni_{1.60}Sn$, in which new Ni_3Sn forms). The c_{HT}/a_{HT} axial ratio of the main HT-$Ni_{1+\delta}Sn$ phase determined from the lattice parameters increases slightly with decreasing annealing temperature (Fig. 3). Remarkably, for the $Ni_{1.60}Sn$-powder alloys, annealing at 673 K show that, besides formation of Ni_3Sn had occurred, also formation of the LT phase with lower Ni content than corresponding to $Ni_{1.60}Sn$ had taken place. This means that three phases (HT, LT, Ni_3Sn) are simultaneously present in these samples, which was not observed for the alloys annealed in the bulk state.

(b) Bulk and powder samples annealed at and quenched from 573 K or lower temperatures give rise to X-ray diffraction patterns which show the same fundamental reflections as observed for the HT phase obtained for higher annealing temperatures. However, the (apparent) hexagonal lattice parameters lead to considerably higher c_{HT}/a_{HT} axial ratios than observed for higher annealing temperatures (Fig. 3). Furthermore, broad additional reflections are observed. These can be indexed as 1st-order satellite reflections $hklm$ ($m = -1, 1$) with respect to an orthorhombic average unit cell $a_{orth} \approx a_{HT}$, $b_{orth} = 3^{1/2} a_{orth}$, $c_{orth} \approx c_{HT}$ (where $3^{1/2} a_{orth} = b_{orth}$ indicates the absence of an orthorhombic distortion of lattice; the lattice is *pseudohexagonal*) and a modulation vector $\mathbf{q} = \alpha \mathbf{a}^*_{orth}$ with $\alpha > 0.5$. The phase showing these features in X-ray powder-diffraction patterns is called LT″ phase. Notably, no further Ni_3Sn and LT phase are formed upon annealing at these temperatures.

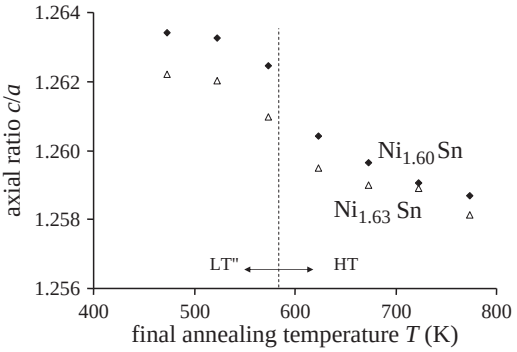

Fig. 3. Annealing-(equilibration-)temperature dependant evolution of the axial ratio c_{HT}/a_{HT} or effective axial ratio of LT″/HT-$Ni_{1.60}Sn$ and LT″/HT-$Ni_{1.63}Sn$ (bulk samples annealed for 1–2 days and powdered before measurement). The dashed line indicates the polymorphic transition temperature (not considering the two-phase region indicated in Fig. 1).

The above-presented results are largely compatible with the phase diagram shown in Fig. 1 [7].[1] However, the 'three-phase' states developing in $Ni_{1.60}Sn$ powders at $573\text{ K}<T<673$ K (HT+LT+Ni_3Sn) cannot correspond to an equilibrium state in the binary Ni–Sn system, which indicates that no complete equilibrium had been attained. This may indicate that metastable phase equilibria occur in the Ni–Sn system and that the constitution of the Ni–Sn system is possibly more complex in this temperature/concentration region than indicated by Ref. [7], e.g. a Ni_3Sn+LT two-phase region might exist.

3.2. Rietveld analysis of the LT″-$Ni_{1.60}Sn$ and line-broadening model

Single-phase HT-$Ni_{1.60}Sn$ powder quenched from 1023 K was transformed into single-phase LT″-$Ni_{1.60}Sn$ by annealing for 10 d at 573 K followed by quenching. X-ray powder-diffraction data of that incommensurate phase were evaluated by the Rietveld method (Fig. 4) in order to quantitatively determine the structure parameters of the LT″ phase.

A major problem for a successful Rietveld analysis of the powder-diffraction data was the considerable and anisotropic diffraction-line broadening of the *satellite* reflections $hklm$ ($m = \pm 1$; see inset of Fig. 4b vs. c), which did not occur for the LT/LT′ specimens analysed in Ref. [5], see, however, end of present section. In contrast, the line profiles of the *fundamental* reflections $hkl0$ could well be described by a pseudo-Voigt function [14] with continuously diffraction-angle (2θ) dependent shape and width parameters (*isotropic* line broadening). This pseudo Voigt function was parametrised employing separately 2θ-dependent Gaussian and Lorentzian line widths [14], allowing for application

[1] Thereby, tolerating minor deviations in the phase boundaries and in the invariant temperatures: (a) The peritectoid temperature of the LT″ phase is located at 568 K in Ref. [7], whereas here annealing at 573 K clearly produced LT″ phase for both $Ni_{1.60}Sn$ and $Ni_{1.63}Sn$. (b) The occurrence of Ni_3Sn precipitation in $Ni_{1.60}Sn$ alloys upon annealing below 1023 K may be understood by a slight shift of the phase boundary HT/Ni_3Sn+HT to lower Ni contents.

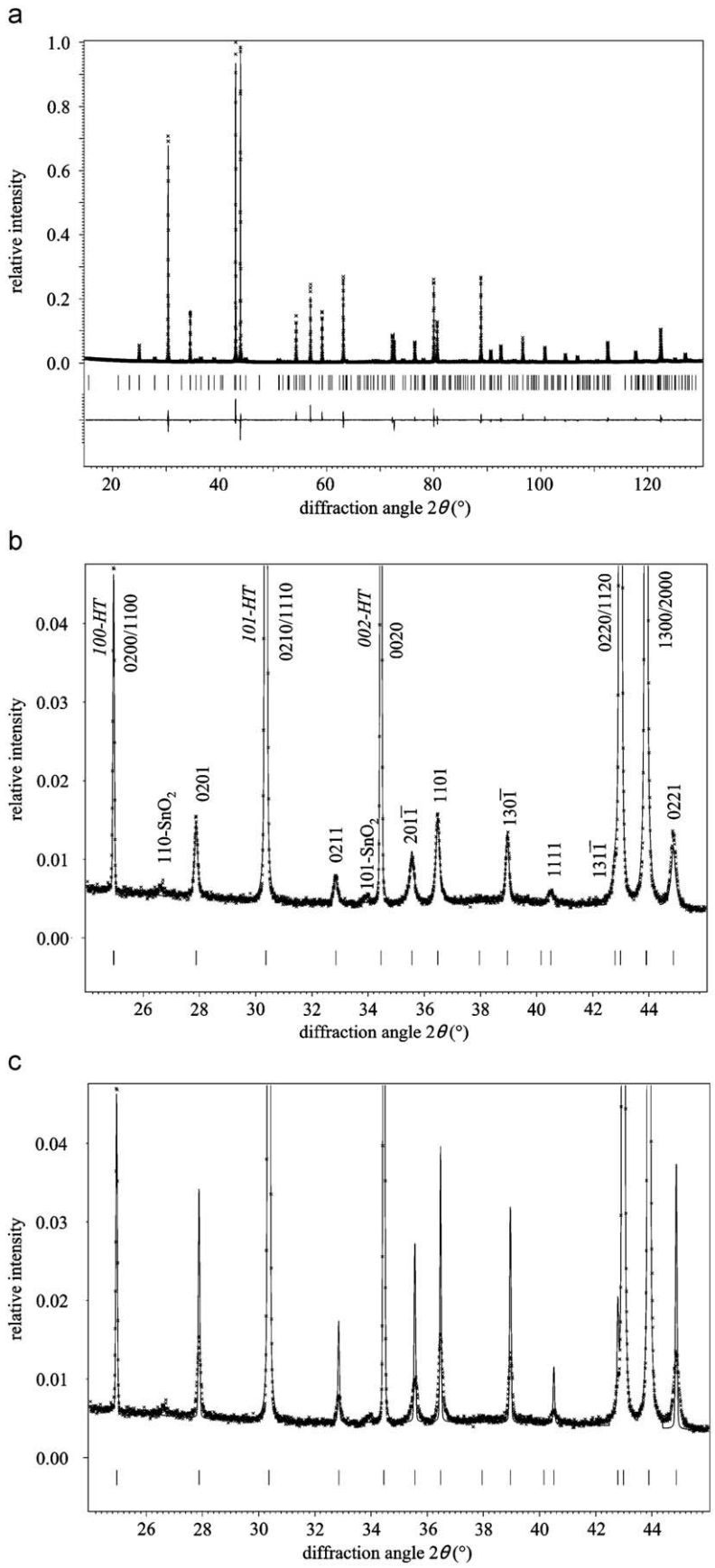

Fig. 4. (a) X-ray powder diffraction pattern (Cu$K\alpha$1 radiation) of incommensurate LT″-$Ni_{1.60}Sn$ (crosses) and calculated diffraction profile (solid line) as the result of a Rietveld refinement of the crystal structure. At the bottom reflection markers (black: fundamental reflections, grey: 1st-order satellite reflections) and the difference curve (observed–calculated intensity) have been indicated. The maximum observed intensity of 62 339 counts corresponds to a relative intensity of 1.0. (b) Enlarged part of (a) without difference curve demonstrating the quality of the fit of the satellite reflections. (c) Same as (b) but calculated pattern after setting S'_{2002}, S'_{0202} and S'_{0022} to 0 (see Eq. (3b); without afterwards refinement leading to too narrow calculated satellite reflections).

of the Voigt function's convolution rules. The line broadening pertaining to the fundamental reflections was adopted as instrumental resolution function.[2]

For the appropriate description of the line-broadening exhibited by the *satellite* reflections a recently developed model designed for incommensurate crystal structures [15] was used as implemented into the programme JANA2006 [13]. Therefore, the above-mentioned isotropic (only 2θ-dependent) pseudo-Voigt function used for description of the *hkl*0 fundamental reflections was convoluted by Gaussian and Lorentzian line-width contributions as given by their full-width-at-half-maximum-values $B_{G,\Delta 2\theta}$ and $B_{L,\Delta 2\theta}$ (in rad):

$$B_{G,\Delta 2\theta}(hklm) = \frac{1-\zeta'}{100}(8\ \ln 2)^{1/2}\ \tan\langle\theta_{hklm}\rangle\langle d^2_{hklm}\rangle\Sigma^{1/2}_{hklm}, \tag{2a}$$

$$B_{L,\Delta 2\theta}(hklm) = \frac{\zeta'}{100}\tan\langle\theta_{hklm}\rangle\langle d^2_{hklm}\rangle\Sigma^{1/2}_{hklm}, \tag{2b}$$

where $\langle d_{hklm}\rangle$ and $\langle\theta_{hklm}\rangle$ are the (average) *d*-spacing and the diffraction-angle of the reflection *hklm*, and where ζ' is a refinable weighing parameter quantifying the Gaussian/Lorentzian character of the line shape of that line-broadening contribution. In Eq. (2) Σ_{hklm} is a 4th-order polynomial in *h*, *k*, *l* and *m*, which reads for the orthorhombic symmetry of LT″ (following the philosophy for prefactors adopted in JANA2006 [13]):

$$\begin{aligned}\Sigma_{hklm} = {} & S'_{4000}(h+\alpha m)^4 + S'_{0040}k^4 + S'_{0040}l^4 \\ & + 6S'_{2200}(h+\alpha m)^2k^2 + 6S'_{2020}(h+\alpha m)^2l^2 \\ & + 6S'_{0220}k^2l^2 + 4S'_{3001}(h+\alpha m)^3m + 12S'_{1201}(h+\alpha m)k^2m \\ & + 12S'_{1021}(h+\alpha m)l^2m + 6S'_{2002}(h+\alpha m)^2m^2 \\ & + 6S'_{0202}k^2m^2 + 6S'_{0022}l^2m^2,\end{aligned} \tag{3a}$$

with the S'_{HKLM} ($H+K+L+M=4$) as refinable line-width parameters. In order to ensure that the line broadening due to Eq. (2) and Eq. (3a) only affects the satellite reflections, only the S'_{HKLM} coefficients with $M=2$ are non-zero, leading to

$$\Sigma_{hklm} = 6S'_{2002}(h+\alpha m)^2m^2 + 6S'_{0202}k^2m^2 + 6S'_{0022}l^2m^2, \tag{3b}$$

so that Σ_{hklm} is non-zero only for satellite reflections, i.e. for $m\neq 0$ (see also footnote 2). Σ_{hklm} would also be non-zero only for $m\neq 0$, however, if additionally the S'_{HKL1} are non-zero. $S'_{HKL1}\neq 0$ is, however, only possible if $S'_{HKL0}\neq 0$ and $S'_{HKL2}\neq 0$ hold simultaneously [15].

Further details concerning the Rietveld analysis are given in Table 1. The crystal-structure model was based on the same average structure and modulation functions as employed for the LT′ phase [5] and is given with the refined model parameters in Table 2. Whereas the results concerning the (atomic) crystal-structure refinement of LT″-$Ni_{1.60}Sn$ will be discussed in Section 3.3, the refined line-width related parameters according to Eqs. (2) and (3b) are discussed in the following.

[2] Note that the "actual" instrumental profile was not quantitatively assessed in this Rietveld analysis. Experience shows that for the present type of $Ni_{1+\delta}Sn$ alloys the line broadening exhibited by fundamental reflections is indeed small compared to the instrumental resolution of the presently used diffractometer. In principle one could also consider the (relatively small) $\tan\theta$-dependent parts of the total line widths or of the additional (with respect to instrumental resolution, i.e. physical) line broadening of the fundamental reflections within the anisotropic line broadening model described in Ref. [15]. This would imply use of complete Eq. (3a) instead of the simplified Eq. (3b). This has, however, several disadvantages in the present case: (a) although the line widths of the fundamental reflections vary in a simple, θ-dependent fashion (i.e. isotropically), many (correlating) S'_{HKL0} (and S'_{HKL1}) parameters are required to model the $\tan\theta$-dependent part of that line broadening. (ii) The physical line broadening of the fundamental reflections may have a different shape than the line broadening of the satellite reflections. This shape variation of the line broadening cannot be considered within the presently used anisotropic line broadening model [15].

Refinement of the line-shape parameter ζ' showed that a broad minimum of the residuals exists close to $\zeta'=1$ (pure Lorentzian broadening) and also that a strong correlation occurs with the width parameters S'_{2002}, S'_{0202} and S'_{0022} so that for the final refinement the value of ζ' was fixed to 1.

For the interpretation of the width parameters it must be emphasised that only 1st-order satellites ($m=\pm 1$) had recognisable intensity so only these could be used directly to determine S'_{2002}, S'_{0202} and S'_{0022}. Although the line-broadening model [15] employed here for the satellite reflections was originally derived assuming a correlated distribution of lattice and modulation parameters, leading basically to something, which can be conceived as *microstrain broadening*, a special case (already basically discussed in Ref. [15]) arises if (as fulfilled here): (i) line broadening occurs only for satellite reflections (narrow fundamental reflections) and (ii) only satellite reflections of a single order are observed, e.g. as here of only 1st-order satellite reflections, i.e. $m=\pm 1$.

In this special case the expression for the line-width according to Eqs. (2b) and (3) is compatible with size-type line broadening for the satellite reflections. This can be shown by equating a combination of Eq. (2b) and (3b) with an expression for Scherrer(size-)-type line broadening, $B_{L,\Delta 2\theta} = 0.9\lambda/D_x\ \cos\langle\theta_{hklm}\rangle$ [20], where $D_{\mathbf{x}}$ is a direction-dependent *effective* crystallite (ordered domain) size measured along the unit vector $\mathbf{x}$ being parallel to the diffraction vector. Inserting $m=\pm 1$ and using Bragg's law, $\lambda = 2\langle d_{hkl\pm 1}\rangle\ \sin\langle\theta_{hkl\pm 1}\rangle$, one obtains:

$$\begin{aligned}&\frac{0.9\times 2\langle d_{hkl\pm 1}\rangle\sin\langle\theta_{hkl\pm 1}\rangle}{D_{\mathbf{x}}\cos\langle\theta_{hkl\pm 1}\rangle} \\ &\quad = \frac{1}{100}\tan\langle\theta_{hkl\pm 1}\rangle\langle d^2_{hkl\pm 1}\rangle(6S'_{2002}(h\pm\alpha)^2 \\ &\qquad + 6S'_{0202}k^2 + 6S'_{0022}l^2)^{1/2},\end{aligned} \tag{4a}$$

$$\frac{1}{D_{\mathbf{x}}} = \frac{1}{180^\circ}\left(\frac{6S'_{2002}(h\pm\alpha)^2 + 6S'_{0202}k^2 + 6S'_{0022}l^2}{\dfrac{(h\pm\alpha)^2}{a^2_{\mathrm{orth}}} + \dfrac{k^2}{b^2_{\mathrm{orth}}} + \dfrac{l^2}{c^2_{\mathrm{orth}}}}\right)^{1/2}. \tag{4b}$$

Eq. (4b) indicates that the observed line broadening of the satellite reflections can indeed be understood as *size broadening* with the effective crystallite size varying continuously as a function of the direction of the diffraction vector

$$\mathbf{x} = ((h\pm\alpha)\mathbf{a}^*_{\mathrm{orth}} + k\mathbf{b}^*_{\mathrm{orth}} + l\mathbf{c}^*_{\mathrm{orth}})/|(h\pm\alpha)\mathbf{a}^*_{\mathrm{orth}} + k\mathbf{b}^*_{\mathrm{orth}} + l\mathbf{c}^*_{\mathrm{orth}}|, \tag{5}$$

whereas this size is constant for a fixed direction of the diffraction vector, as required for size broadening.

The values thus obtained for the effective size $D_{\mathbf{x}}$ along the three crystallographic directions of high symmetry are (requiring transformation of the S' values into radian units):

along $[100]_{\mathrm{orth}}$:

$$D_{\mathbf{x}\parallel\mathbf{a}^*_{\mathrm{orth}}} = 180^\circ(6a^2S'_{2002})^{-1/2} \approx 670\ \text{Å}, \tag{5a}$$

along $[010]_{\mathrm{orth}}$:

$$D_{\mathbf{x}\parallel\mathbf{b}^*_{\mathrm{orth}}} = 180^\circ(6b^2S'_{0202})^{-1/2} \approx 850\ \text{Å}, \tag{5b}$$

along $[001]_{\mathrm{orth}}$:

$$D_{\mathbf{x}\parallel\mathbf{c}^*_{\mathrm{orth}}} = 180^\circ(6c^2S'_{0022})^{-1/2} \approx 440\ \text{Å}. \tag{5c}$$

The occurrence of size-like line broadening of the 1st-order satellite reflections can be understood as follows: The complete volume of the original HT-phase crystals is transformed into the orthorhombic LT″ phase. However, this LT″-phase microstructure does not consist of one single domain but is composed from small,

Table 1
Details of the X-ray powder-diffraction experiment and the corresponding Rietveld refinement of LT″-$Ni_{1.60}Sn$.

Diffractometer	Philips/Panalytical X'Pert MPD, Cu anode, Ge Johannson-type monochromator in the primary beam, $\lambda = 1.54056$ Å
Detector	Position sensitive detector X'Celerator covering 2.2° on the 2θ scale
No. of recorded reflections[a]	83 fundamental ($m = 0$) 147 satellite ($m = \pm 1$)
Recorded diffraction angle range, stepwidth (°) number of data points	15.001–129.994, 0.009 12778
Software	JANA2006 [13]
Profile function for fundamental reflections	Thompson–Cox–Hastings version of the pseudo-Voigt function [14] (five parameters) Instrumental asymmetry correction [16] (one parameter)
Peak profile parameters for line broadening of satellite reflections [15]	
S'_{2002} (°/Å^2)^2	2.3(1)
S'_{0202} (°/Å^2)^2	0.48(3)
S'_{0022} (°/Å^2)^2	3.4(2)
ζ'	1(–)
Absorption correction	Surface roughness, two parameters [17]
No. of background parameters (Legendre polynomials)	16
Refined zero shift (°)	−0.0614(3)
Lattice parameters	
a_{orth} (Å) ($\approx a_{hcp}$)	4.12682(3)
b_{orth} (Å) ($\approx 3^{1/2} a_{HT}$)	7.14936(6)
c_{orth} (Å) ($= c_{hcp}$)	5.20998(2)
Modulation parameter α	0.57139(4)
Orthorhombic distortion $orth = b_{orth}/3^{1/2}a_{orth} - 1$	0.00021(1), must be regarded as insignificantly small[b]
effective axial ratio $c_{HT}/a_{HT} = c_{orth}/(a_{orth}b_{orth}/3^{1/2})^{1/2}$	1.262336(2)
Residuals [18]	$R_{wp} = 9.33$, $R_p = 6.58$
R_{Bragg}(satellites) = 4.07	R_{Bragg}(main reflections) = 3.44
Berar's factor [19]	2.9

Numbers in parentheses indicate the standard deviations determined by the Rietveld refinement, where (–) indicates that an in principle refinable parameter was held fixed for a reasons discussed in the text.

[a] Only satellite reflections with $m = \pm 1$ were considered for the *calculated* patterns.

[b] No reflection splitting due to the orthorhombic symmetry can be discerned. Test refinements enforcing $b_{orth} = 3^{1/2}a_{orth}$ (pseudohexagonality of the lattice) lead only to a marginal increase of the residuals, indicating that the deviation of the parameter *orth* from 0 is an artifact of the refinement.

Table 2
Incommensurately modulated structure model for LT″-$Ni_{1.60}Sn$ with $Cmcm(\alpha 00)0s0$ symmetry as used in the course of the Rietveld refinement.

Average structure of the LT and LT′ phases: $Cmcm$, $a_{orth} \approx a_{HT}$, $b_{orth} \approx 3^{1/2}a_{HT}$, $c_{orth} \approx c_{HT}$ (see also Table 1)

M	x^M_{av}	y^M_{av}	z^M_{av}	Occupancy
Sn	0	y^{Sn}_{av}	$\frac{1}{4}$	1
Ni(1)	0	0	0	1
Ni(2)	0	$y^{Ni(2)}_{av}$	$\frac{1}{4}$	δ (with respect to $Ni_{1+\delta}Sn$)

Final coordinates and occupancies of the atoms as resulting from the average structure and the modulation functions, refined parameters[a].

Additionally in { } the refined parameters obtained for LT′-$Ni_{1.41}Sn$ equilibrated at 473 K [5] are given.

Sn

$x_{Sn} = u^{Sn}_{x,c,1} \cos 2\pi x_4 + u^{Sn}_{x,s,2} \sin 4\pi x_4 + u^{Sn}_{x,c,3} \cos 6\pi x_4$, $y_{Sn} = y^{Sn}_{av} + u^{Sn}_{y,s,1} \sin 2\pi x_4 + u^{Sn}_{y,c,2} \cos 4\pi x_4 + u^{Sn}_{y,s,3} \sin 6\pi x_4$

$z^{Sn} = \frac{1}{4}$, $occ^{Sn} = 1$

With

$u^{Sn}_{x,c,1} = -0.0411(3)\{-0.0494(5)\}$, $u^{Sn}_{x,s,2} = -0.0231(6)\{-0.0172(6)\}$, $u^{Sn}_{x,c,3} = 0.034(1)\{0.023(1)\}$

$y^{Sn}_{av} = 0.3334(2)\{0.3305\}$, $u^{Sn}_{y,s,1} = -0.0207(1)\{-0.0221\}$, $u^{Sn}_{y,c,2} = 0.0144(8)\{0.0048\}$, $u^{Sn}_{y,s,3} = -0.0176(5)\{0.004\}$

atomic displacement parameter $\langle u^2_{Sn}\rangle = -0.0017(5)$ Å^{2,b} $\{0.0127(4)\}$

Ni(1)

$x^{Ni(1)} = u^{Ni(1)}_{x,s,2} \sin 4\pi x_4$, $y^{Ni(1)} = u^{Ni(1)}_{y,s,1} \sin 2\pi x_4$, $z^{Ni(1)} = u^{Ni(1)}_{z,s,1} \sin 2\pi x_4$, $occ^{Ni(1)} = 1$

With

$u^{Ni(1)}_{x,s,2} = 0.001(5)\{0.004(2)\}$, $u^{Ni(1)}_{y,s,1} = -0.0131(3)\{-0.0195(5)\}$, $u^{Ni(1)}_{z,s,1} = 0.0002(5)\{0.0056(7)\}$

atomic displacement parameter $\langle u^2_{Ni(1)}\rangle = 0.0033(5)$ Å^2 $\{0.0127(5)\}$

Ni(2)

$x^{Ni(2)} = 0 + u^{Ni(2)}_{x,c,1} \cos 2\pi x_4$, $y^{Ni(2)} = y^{Ni(2)}_{av}$, $z^{Ni(2)} = \frac{1}{4}$, $occ^{Ni(2)} = \delta + p^{Ni(2)}_{s,1} \sin 2\pi x_4$

with

$\delta = 0.600(-)$ $\{0.409(-)\}$

$p^{Ni(2)}_{s,1} = 0.440(5)\{0.531(6)\}$, $u^{Ni(2)}_{x,c,1} = 0.0092(8)\{0.001(2)\}$, $y^{Ni(2)}_{av} = 0.6579(4)\{0.6558(6)\}$,

atomic displacement parameter $\langle u^2_{Ni(2)}\rangle = \langle u^2_{Ni(1)}\rangle$

Numbers in parentheses indicate the standard deviations determined in the course of the Rietveld refinement, where (–) indicates that an in principle refinable parameter was held fixed for a certain reasons.

[a] $x_4 = t + \alpha \times (x_{av} + T_x)$, where t is the global phase of the modulation wave, and where x_{av} is the average x position of the atom in the average unit cell and where T_x is the component of a translation vector parallel to the [100] direction of the average unit cell. The modulation parameters are: displacement parameters u with subscripts (x, y, z) indicating the direction of the modulation, and occupational parameters p. The subscripts s and c denote that the modulation parameters refer to a sine or cosine term and the subscript numbers indicates the harmonic order of the modulation function.

[b] This physically unreasonable negative atomic displacement parameter may e.g. be caused by incomplete consideration of absorption effects related with surface roughness of the specimen, since there is a strong correlation between the refined surface-roughness parameters and the atomic displacement parameters.

differently oriented—with respect to the hexagonal HT structure—(twin) domains and from domains separated by anti-phase boundaries. The limited size of these domains leads to size-broadening for the satellite reflections. However, the fundamental reflections remain unbroadened, because, due to the pseudo-hexagonal lattice parameters, the basic structure of the differently oriented domains diffracts coherently. Indeed, for LT-$Ni_{1.50}Sn$ a similar line broadening affecting the superstructure reflections (analogues of the satellite reflections in LT″) was also observed if the ordering was induced by annealing at temperatures considerably below the ordering temperature. At later stages of annealing, the orthorhombic distortion develops in LT-$Ni_{1.50}Sn$ leading to more complicated line-broadening phenomena also for the fundamental reflections, which become finally split [21,22], which is not the case for LT″, see also Section 3.3.4.

Note that the present line-broadening model would not be applicable if second- or higher-order satellites experiencing the domain-size broadening were present with detectable intensity in the powder-diffraction pattern.

3.3. The structural properties of LT″-$Ni_{1.60}Sn$ compared with those of LT′ and LT

3.3.1. General remarks

The modulated crystal structure of the incommensurate LT″-$Ni_{1+\delta}Sn$ phase shows similarity with those of the incommensurate LT′-$Ni_{1+\delta}Sn$ phase and of the commensurate LT-$Ni_{1+\delta}Sn$ phase [5] (see, however, also Section 3.3.4). This similarity is already indicated by the fact that all three phases have the same (with respect to the HT phase cell) type of average unit cell $a_{orth} \approx a_{HT}$, $b_{orth} \approx 3^{1/2} a_{HT}$, $c_{orth} \approx c_{HT}$, that they have similar modulation vectors $\mathbf{q} = \alpha \mathbf{a}^*_{orth}$ with $\alpha > \frac{1}{2}$ for LT″, $\alpha = \frac{1}{2}$ for LT and $\alpha < \frac{1}{2}$ for LT′ and that they can be described with the same superspace-group symmetry $Cmcm(\alpha 00)0s0$. Furthermore, the same occupational (for Ni(2)) and displacive modulation functions can be employed for structure refinement of incommensurate LT″-$Ni_{1.60}Sn$ as previously successfully employed for incommensurate LT′-$Ni_{1+\delta}Sn$ ($0.35 \leqslant \delta \leqslant 0.41$) and in a similar form for commensurate LT-$Ni_{1+\delta}Sn$ ($Ni_{1.47}Sn$ and $Ni_{1.50}Sn$) [5]. In fact, although there are marked differences between the LT′ and LT″ phases (see Section 3.3.4), one may in principle conceive the LT phase to disrupt as a lock-in phase a hypothetical single incommensurate phase comprising at low temperatures the composition ranges of the whole $Ni_{1+\delta}Sn$ 'phase region' (of which the LT′ and LT″ are the remainders). Nevertheless, due to the necessary 1st-order character of the lock-in transitions LT″ ⇄ LT and LT ⇄ LT′ (with necessary occurrence of two-phase fields; already mentioned in Ref. [7]), LT, LT′ and LT″ must be conceived as three individual ordered phases.

Unfortunately, the direct and quantitative interpretation of the structure parameters of LT″-$Ni_{1.60}Sn$ as obtained by Rietveld refinement, is hampered by a problem similar to that met previously for the LT′ phase [5]. For occupational modulation functions often a 1st-order harmonic function as employed here for refinement ($occ^{Ni(2)} = \delta + p^{Ni(2)}_{s,1} \sin 2\pi x_4$; also employed for LT′) is not sufficient to describe the real occupational modulation. However, reliable refinement of higher-order occupational modulation parameters (here $p^{Ni(2)}_{c,2}$, $p^{Ni(2)}_{s,3}$) usually requires measurement of the intensities of higher-order satellite reflections, which are, however, not observed and probably too weak in the presently available powder-diffraction pattern. If the occupation modulation would be ideal (occupancies of 0 or 1 for Ni(2) everywhere in the crystal structure), an alternative to a high-order series of harmonic function would be provided by Crenel functions [23]. However, like for the LT′-$Ni_{1+\delta}Sn$ phase [5], it can shown that the value refined here for $p^{Ni(2)}_{s,1}$ is far too low to be compatible with a Crenel-like occupational modulation of Ni(2). Thus in the crystal structure occupancies intermediate between 0 and 1 occur, implying partial disorder and superposition of different atomic arrangements in the crystal structure. E.g. interatomic distances around regions of the crystal structure close to intermediately occupied Ni(2) sites must be interpreted with care (see e.g. analysis of apparently extremely short Ni(2)–Sn distances, which can be obtained from a superficial crystal-structure analysis of HT-$Ni_{1+\delta}Sn$ [6]).

3.3.2. Occupational modulation

In agreement with the systematic variation with composition of the parameter α describing the length of the modulation vector $\mathbf{q} = \alpha \mathbf{a}^*_{orth}$ as indicated in Fig. 5 for the LT″, LT and LT′ phases, the ordered distribution of Ni(2) in the Sn_5-trigonal–bipyramidal interstices varies systematically as a function of composition. As already indicated in Section 3.3.1, the refined value for the occupational modulation-amplitude parameter $p^{Ni(2)}_{s,1}$ indicates that in comparison with an ideal Crenel-type occupational ordering the long-range ordering in LT″-$Ni_{1.60}Sn$ is incomplete, like in the LT′ phase, for which also a significant variation of $p^{Ni(2)}_{s,1}$ with the (equilibration) annealing temperature was observed [5]. In contrast, the long-range ordering of Ni(2) in the commensurate LT phase (see Fig. 6a) was found to be virtually complete, at least after equilibration temperatures of $\leqslant 673$ K.

In order to illustrate the Ni(2) distributions for the partially disordered LT″ phase by an atomic-structure models of LT″-$Ni_{1.60}Sn$ only the Ni(2) having an occupancy larger than $\frac{1}{2}$ ('cut-off occupancy') are drawn (Fig. 6b) using the *Graphics Output* feature of JANA2006 [13].

The discussion of the Ni(2) distribution in the ordered LT″-$Ni_{1+\delta}Sn$ phase may depart from than in ideal LT-$Ni_{1.50}Sn$ (Ni_3Sn_2, Fig. 6a), in which exactly $\frac{1}{2}$ of the trigonal–bipyramidal sites are occupied. One recognises Ni(2) *zig-zag chains* running parallel to b_{orth}, which are separated by similar *vacancy-zig-zag chains* (empty trigonal–bipyramidal sites). The *increase* of the Ni(2) content (with respect to LT-$Ni_{1.50}Sn$) in the LT″ phase is realised by a *removal* of vacancies from the *vacancy-zig-zag chains* so that the average separation distance between the Ni(2) *zig-zag chains decreases*, which is reflected by an *increase* of the modulation parameter α (Fig. 5) and, by that, by an *elongation* of the modulation vector (Fig. 6b). As already indicated in Ref. [5] the *decrease* of the Ni(2) content (i.e. of δ, with respect to LT-$Ni_{1.50}Sn$) upon going towards the low-Ni(2)-content LT′ phase, is realised by a systematic *introduction* of *additional* vacancies which *increases*

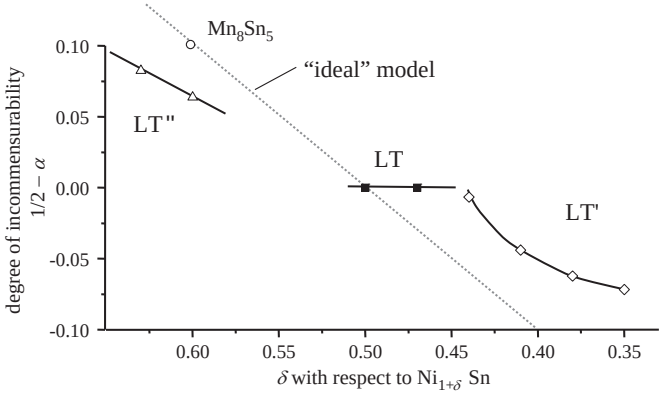

Fig. 5. Variation of the modulation parameter α determining the length of the modulation vector $\mathbf{q} = \alpha \mathbf{a}^*_{orth}$ with respect to the reciprocal lattice basis vectors of the average structure (index orth).

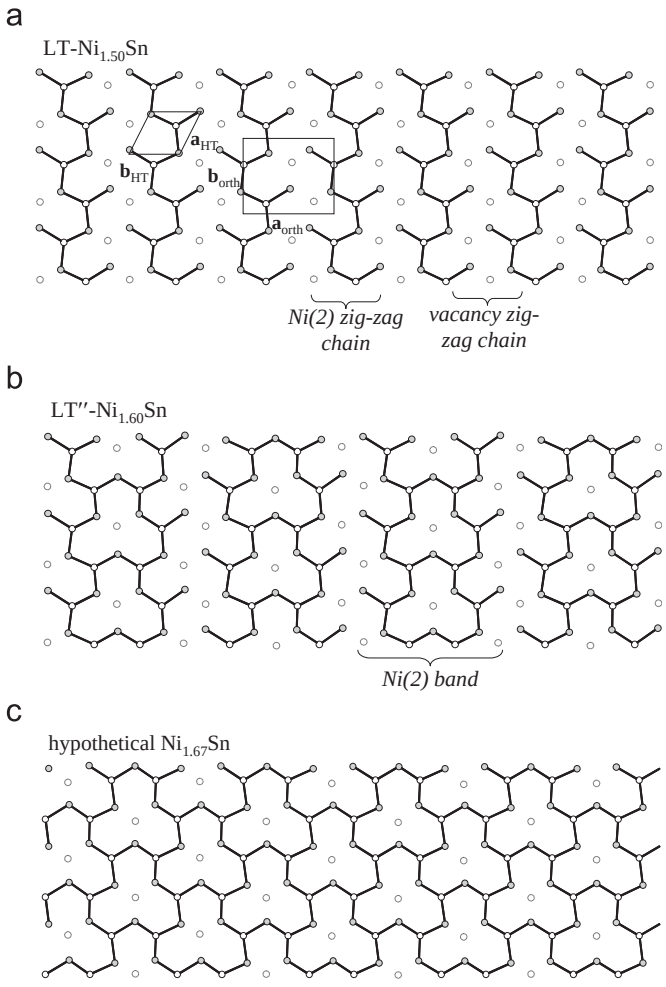

Fig. 6. Ni(2) distributions in an Ni(2)–Sn layer at $z=\frac{1}{4}$ in (a) ideal commensurate LT-$Ni_{1.50}Sn$ and (b) incommensurate LT″-$Ni_{1.60}Sn$ as given in Table 2, the latter calculated as approximant structure using the *Graphics Output* feature of JANA2006, assuming Ni(2) sites with occupancies >0.5 to be occupied and the others to be empty (see text). Unit cells of the hexagonal HT phase and of the orthorhombic average structure have been indicated. 'Bonds' Ni(2)–Sn correspond to the expanded basal Ni(2)–Sn distances also shown in Fig. 2. (c) Similar Ni(2) distribution resulting for hypothetical state with $\alpha=\delta=\frac{2}{3}$ ('$Ni_{1.67}Sn$' or 'Ni_5Sn_3'; occurring in reality in Ni_5Ge_3 [26]) exhibiting (local) threefold rotational symmetry in this Ni(2)–Sn plane.

the average separation distance between the Ni(2) *zig-zag chains* (corresponding to the maxima in the occupational modulation function). This is reflected by the decrease of the modulation parameter α (Fig. 5) and thus by a *contraction* of the wave vector $\mathbf{q}=\alpha\mathbf{a}^*_{orth}$ of the occupational modulation wave.

It was previously shown [5] that for an idealised structure model based on a Crenel-like incommensurate ordering of Ni(2) the modulation parameter α can be related with the average occupancy δ of the Ni(2) sites: $\alpha=\delta$. However, in experimental reality this relation is obeyed only for $\alpha=\delta=\frac{1}{2}$ (for ideal LT-$Ni_{1.50}Sn$). For the LT′ [5] and LT″ phases (as observed here) the value of α is found to be closer to $\frac{1}{2}$ than as given by $\alpha=\delta$ (Fig. 5). This may be explained by the incomplete degree of occupational ordering of Ni(2). Indeed, $Mn_{1.60}Sn$ (Mn_8Sn_5)—having the same superspace group and following the same structural building principles as the ordered $Ni_{1+\delta}Sn$ phases—exhibits ideal Crenel-like incommensurate ordering of Mn(2) (named analogous to Ni(2)) and follows $\alpha\approx\delta=0.6$ [24], which is not the case for LT″-$Ni_{1.60}Sn$ ($\alpha\approx0.57$) having the same δ value as $Mn_{1.60}Sn$ (see Fig. 5).

3.3.3. *Atomic displacements accompanying occupational modulation*

Already for the LT and LT′ phases [5] analysis of the structure changes with respect to the parent HT phase had shown that characteristic lattice strains and displacements of the atoms from their ideal positions occur with reference to the HT phase (deviations from $y^{Sn}_{av}=\frac{1}{3}$ and $y^{Ni(2)}_{av}=\frac{2}{3}$ as well as displacement modulations). These structure changes can be conceived to be caused by the occupational modulation of Ni(2). The most prominent factor determining these lattice strains and displacements is the space requirements of the Ni(2) atoms in the occupied Sn_5-trigonal bipyramids. The presence of a Ni(2) atom in a Sn_5-trigonal bipyramid leads in particular to strong displacements of Sn in *x* and *y* directions relieving otherwise unrealistically short (2.3–2.4 Å) Ni(2)–Sn distances in the Sn_3-basal planes of the occupied trigonal bipyramids to result in reasonable values of 2.5–2.6 Å. The empty trigonal bipyramids become contracted in their basal plane (see Fig. 2b).

In the LT″ phase similar displacement modulations occur as in the LT′ phase, compare values of the structure parameters for LT″-$Ni_{1.60}Sn$ and LT′-$Ni_{1.41}Sn$ as given in Table 2. The effect of the displacement parameters is illustrated here by plotting the variation of the Ni(2)–Sn distances vs. the internal coordinate *t* in Fig. 7, where Ni(2) sites with an occupancy below 0.5 ('cut-off occupancy') are regarded as unoccupied and above 0.5 are regarded as occupied (the employed occupancy modulation function is in fact sinusoidal, see Table 2). Thus the Ni(2)–Sn distances in the *t* regime with occupied Ni(2) are regarded to exist, those in the *t* regime with unoccupied Ni(2) are regarded not to exist; the latter distances may be regarded as distances from the centre of an unoccupied trigonal bipyramid to the nearest-neighbour Sn atoms. In fact, with respect to a mean Ni(2)–Sn basal distance of 2.38 Å (corresponding to $3^{-1/2}a_{HT}$) the Ni(2)–Sn distances in the occupied trigonal bipyramids are considerably expanded. Slightly unrealistically short Ni(2)–Sn distances close to the transition from the occupied Ni(2) to the unoccupied Ni(2) *t*-regime must be related with the limited information provided by the 1st-order satellite reflections and with the partial disorder in the Ni(2) distribution (see Section 3.3.1).

3.3.4. *"Compositional asymmetry" of the ordering in the* $Ni_{1+\delta}Sn$ *phases*

Having a common superspace-group symmetry *Cmcm*(α00)0*s*0, the three different ordered $Ni_{1+\delta}Sn$ phases occur for different characteristic ranges of the compositional parameter δ and of the modulation parameter α:

LT′: $\delta<0.5$; $\alpha<0.5$

LT: $\delta\approx0.5$; $\alpha=0.5$

LT″: $\delta>0.5$; $\alpha>0.5$

Furthermore, the character of the occupational and displacive modulations is similar in all three phases (see Sections 3.3.2 and 3.3.3).

In spite of the somewhat continuous ordering tendency and the somewhat symmetrical behaviour of the LT′ and LT″ phases on the low-Ni-content and high-Ni-content sides of the composition $Ni_{1.50}Sn/Ni_3Sn_2$, there are also some structural features related with the ordering, which behave *asymmetrically* with respect to the composition $Ni_{1.50}Sn/Ni_3Sn_2$:

(a) There is no significant orthorhombic lattice distortion in the LT″ phase (see Table 2). The fundamental reflections can be indexed with respect to a hexagonal lattice, and also the satellite reflections do not provide sufficient information to detect a significant deviation from *orth* = 0, see Table 1. This is

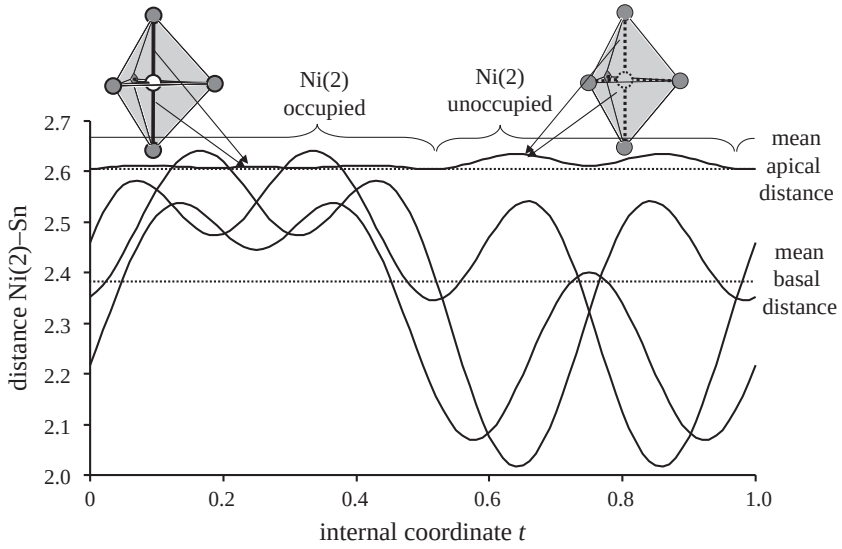

Fig. 7. Plot of the distance Ni(2)–Sn (within Sn_5-trigonal bipyramids) vs. the internal coordinate t in LT″-$Ni_{1.60}Sn$. Curly breaks indicate the t ranges with 'occupied' (occupancy of Ni(2) >0.5) and 'unoccupied' (occupancy of Ni(2)$\leqslant 0.5$) sites due to the sinusoidal occupation modulation of Ni(2). The mean (see text) Ni(2)-Sn apical and basal distances distance have been indicated as dashed lines.

in contrast with the LT and LT′ phases, where *orth* values up to 0.01 are found [5].[3]

(b) It is very difficult to coarsen the LT″-phase domains to yield a large domain size by annealing. The satellite reflections are still broad after considerable annealing times (see Fig. 4), which does not hold for the LT′ phase [5].

(c) For a given deviation from the ideal composition $Ni_{1.50}Sn$, the temperature of the T_t order–disorder transition LT, LT′, LT″ ⇄ HT tends to be lower for high Ni contents (LT″ regime) than for low Ni contents (LT′ regime), see also Fig. 1. The maximum transition temperature does not occur for $\delta = 0.50$ but for slightly lower Ni contents [7].

During coarsening, strain energy of the orthorhombically distorted domains is released. In the absence of an orthorhombic lattice distortion as in LT″ the thermodynamic driving force for coarsening is likely lower than in the case of the presence of an orthorhombic distortion. Thus the relative difficulty to coarsen the ordered domains in pseudohexagonal LT″ is plausible. Moreover, the tendency to establish a significant orthorhombic distortion in LT and LT′ may indicate that the atomic arrangement is optimised within the orthorhombic domains. Thus the lack of an orthorhombic distortion may indicate for LT″ the absence of such optimised arrangements and thus a lower ordering energy. Indeed this would explain the (compared to LT and LT′) low ordering temperature T_t of LT″ (see Fig. 1).

Thus, the key feature making LT″ special compared to LT and LT′ is the absence of the orthorhombic distortion (a), which is the origin of the two other special features of LT″, i.e. the difficulty of domain coarsening (b) and the low ordering temperature (c). Consequently, one may try to understand, which structural factor in the LT″ phase causes the absence (or very small) orthorhombic distortion.

In Ref. [5] the significantly non-zero orthorhombic lattice distortion *orth* (compare Eq. (1)) in the LT/LT′ phases and in particular its positive sign was ascribed to the spatial requirements of the Ni(2) *zig-zag* chains running along b_{orth}. Due to this the b_{orth} axis is expanded, whereas the a_{orth} axis is compressed due to the *vacancy-zig-zag chains* (in trigonal bipyramids; Fig. 6a). These persist and are even extended, by additional vacancies in the LT′ phase (i.e. for low Ni contents/low δ) so that also this phase will exhibit a similar (or even larger) lattice orthorhombicity as the LT phase [5]. Contrary, in the LT″ phase, i.e. for high Ni contents/high δ values, the Ni(2) *zig-zag chains* start to condense to *bands* (Fig. 6b) due to the systematic removal of vacancies from the *vacancy-zig-zag chains* separating the Ni(2) *zig-zag chains*. These *bands* are expected to be more rigid in the a_{orth} direction. Thus one may expect that the value of *orth* is smaller in the LT″ phase, with its Ni(2) *bands*, than in the LT/LT′ phases, which is compatible with the observed pseudo-hexagonal lattice of the LT″ phase (the same arguments hold for ordered Mn_3Sn_2 clearly exhibiting a orthorhombic lattice distortion [25] and orthorhombic-pseudohexagonal $Mn_8Sn_5/Mn_{1.60}Sn$ [24]). Indeed, if one half of the vacancies are removed from the *vacancy-zig-zag* chains, one arrives at an Ni(2) distribution, which is hexagonal within one single Ni(2)–Sn layer (Fig. 6c). For such a layer (alone) no lattice distortion (within such a layer) is expected. Indeed, Ni_5Ge_3 ($Ni_{1.67}Ge$) [26], being also an ordered Ni_2In/NiAs type variant, contains exclusively such layers in its monoclinic superstructure with the (mutually perpendicular) basis vectors $\mathbf{a}_m$ and $\mathbf{b}_m$ being located parallel to the a_{HT}–b_{HT} plane of the parent disordered HT phase. With $a_m \approx 3a_{HT}$ and $b_m = 3^{1/2}a_{HT}$ one can calculate for Ni_5Ge_3 a distortion parameter similar to *orth* (Eq. (1)) $orth' = 3^{1/2}b_m/a_m - 1$ yielding a value of -0.001, which is—if at all significantly larger than zero—much smaller than the *orth* values observed for LT and LT′.

4. Conclusion

(i) Besides the previously reported [5] ordered NiAs/Ni_2In-type $Ni_{1+\delta}Sn$ phases, LT ($\delta \approx 0.5$) and LT′ ($\delta < 0.5$), a third phase LT″ ($\delta > 0.5$) exists. All three phases can be regarded as modulated structures with an occupation modulation of Ni atoms

[3] One might remark that also the LT phase forms initially without exhibiting a clear orthorhombic distortion, as e.g. reported in Ref. [21]. However, already for domain sizes smaller than those found here for LT″-$Ni_{1.60}Sn$ annealed for 10 d at 573 K (see Section 3.2) LT-$Ni_{1.50}Sn$ clearly exhibits orthorhombic lattice distortion by fundamental reflection splitting [22, unpublished data].

accompanied by characteristic atomic-displacement modulations. The superspace-group symmetry is always *Cmcm*(α00) 0*s*0 with LT being commensurate with $\alpha = 0.5$, LT′ and LT″ being incommensurate with $\alpha < 0.5$ and $\alpha > 0.5$, respectively.

(ii) Significant diffraction-line broadening of the satellite reflections is indicative of small ordered-domain size. Employing a newly developed diffraction-line broadening model [15] anisotropic effective domain sizes of 440–850 Å (depending on the crystallographic direction) were determined.

(iii) In spite of common, as a function of composition continuously changing structural features of the ordered $Ni_{1+\delta}Sn$ phases (see point (i)), the LT″ phase shows compared to LT and LT′ some special features. The key feature is a pseudohexagonal lattice (absent orthorhombic distortion), which is connected with condensation of special structure elements in the ordering pattern of Ni in LT″ (Ni(2)-*zig-zag chains*). This condensation does not occur for metrically orthorhombic LT and LT′.

Acknowledgements

The author wishes to thank Dr. V. Petricek (Academy of Sciences of the Czech Republic, Prague, Czech Republic) and Mag. C. Schmetterer and Prof. H. Flandorfer (Institut für Anorganische Chemie und Materialchemie, Universität Wien, Austria) for valuable discussions and Prof. Dr. E.J. Mittemeijer (MPI for Metals Research, Stuttgart, D) for his continuous support of and interest in this work and for his critical reading of the manuscript.

References

[1] P. Nash, A. Nash, Bull. Alloy Phase Diagr. 6 (1985) 350–359.
[2] S. Lidin, Acta Crystallogr. B 54 (1998) 97–108.
[3] S. Lidin, A.-K. Larsson, J. Solid State Chem. 118 (1995) 313–322.
[4] A. Leineweber, M. Ellner, E.J. Mittemeijer, J. Solid State Chem. 159 (2001) 191–197.
[5] A. Leineweber, J. Solid State Chem. 177 (2004) 1197–1212.
[6] A. Leineweber, O. Oeckler, U. Zachwieja, J. Solid State Chem. 177 (2004) 936–945.
[7] C. Schmetterer, H. Flandorfer, K.W. Richter, U. Saeed, M. Kauffman, P. Roussel, H. Ipser, Intermetallics 15 (2007) 869–884.
[8] A.-K. Larsson, R.L. Withers, L. Stenberg, J. Solid State Chem. 127 (1996) 222–230.
[9] M. Ellner, J. Less-Common Met. 48 (1976) 21–52.
[10] H. Fjellvåg, A. Kjekshus, Acta Chem. Scand. A 40 (1986) 23–30.
[11] P. Brand, Z. Anorg. Allg. Chem. 353 (1967) 270–280.
[12] A. Arakcheeva, P. Pattison, G. Chapuis, M. Rossell, A. Filaretov, V. Morozov, G. Van Tendeloo, Acta Crystallogr. B 64 (2008) 160–171.
[13] V. Petricek, M. Dusek, L. Patatinus, JANA2006, The crystallographic computing system, Institute of Physics, Praha, Czech Republic, 2006.
[14] P. Thompson, D.E. Cox, J.B. Hastings, J. Appl. Crystallogr. 20 (1987) 79–83.
[15] A. Leineweber, V. Petricek, J. Appl. Crystallogr. 40 (2007) 1027–1034.
[16] C.J. Howard, J. Appl. Crystallogr. 15 (1982) 615–620.
[17] W. Pitschke, N. Mattern, H. Hermann, Powder Diffr. 8 (1993) 223–228.
[18] R.A. Young, The Rietveld Method, in: R.A. Young (Ed.), Oxford University Press, 1993, pp. 1–38.
[19] J.-F. Bérar, P. Lelann, J. Appl. Crystallogr. 24 (1991) 1–5.
[20] A. Guinier, X-Ray Diffraction in Crystals, Imperfect Crystals and Amorphous Bodies, W.H. Freeman, San Francisco, USA, 1963.
[21] A. Leineweber, E.J. Mittemeijer, M. Knapp, C. Baehtz, Philos. Mag. 87 (2007) 1821–1844.
[22] A. Leineweber, E.J. Mittemeijer, Z. Kristallogr. Suppl. 23 (2006) 351–356.
[23] V. Petricek, V. van der Lee, M. Evain, Acta Crystallogr. A 51 (1995) 529–535.
[24] M. Elding-Pontén, L. Stenberg, S. Lidin, G. Madariaga, J.-M. Pérez Mato, Acta Crystallogr. B 53 (1997) 364–372.
[25] M. Stange, H. Fjellvåg, S. Furuseth, B.C. Hauback, J. Alloys. Compd. 259 (1997) 140–144.
[26] M. Ellner, T. Gödecke, K. Schubert, J. Less-Common Met. 24 (1971) 23–40.